Journal of Solid State Chemistry **147,** 609–617 (1999)
Article ID jssc.1999.8424, available online at http://www.idealibrary.com on IDEAL®

Site Preference of Fe and V in $PbFe_xV_{6-x}O_{11}$ by Neutron Diffraction and Mössbauer Spectroscopy: Low Temperature Investigation for $x = 1.75$

A. C. Dhaussy, O. Mentre,[1] and F. Abraham

Laboratoire de Cristallochimie et Physicochimie du Solide, UPRES A CNRS 8012, ENSCL, Université des Sciences et Technologies de Lille, BP 108, 59652 Villeneuve d'Ascq Cedex, France

and

Y. Calage

Laboratoire des Fluorures, UPRES A CNRS 6010, et Laboratoire de Physique de l'Etat Condensé, UPRES A CNRS 6087, Faculté des Sciences, Université du Mans, Avenue Olivier Messiaen, BP 535, 72085 Le Mans Cedex, France

Received March 18, 1999; in revised form June 4, 1999; accepted June 8, 1999

The $PbFe_xV_{6-x}O_{11}$ series adopting the *R* block structural type were investigated by both powder neutron diffraction and Mössbauer spectroscopy in order to quantify a Fe^{3+} cation occupancy in available crystallographic sites. Four samples with formal *x* ratio of 1, 1.21, 1.6, and 1.75 were investigated. The results obtained from the two techniques match rather well, providing reliable refinements. The preferential vanadium substitution by iron is clearly indicated in *M*(4) triangular bipyramidal sites, while *M*(2) and *M*(3) dimers are statistically occupied by Fe and V. Finally, the layers of octahedral *M*(1) sites remain solely occupied by vanadium. For the latter, Mössbauer and neutron diffraction results slightly diverge because of the possible consideration of iron species within impurities present in the samples. The 2 K crystal structure refinement for $PbFe_{1.75}V_{4.25}O_{11}$ is similar to that of the room temperature form, although there is a surprising *c* stacking axis increase. We have already described the magnetic ZFC/FC strong irreversibility in these series and assigned it to frustration arising in $M(1)O_6$ layers. The magnetic structure refinement confirmed this model as possible in an identical magnetic/crystallographic unit cell.

INTRODUCTION

The crystal structure of the *R*-block type PbV_6O_{11}, a new lead V^{3+}–V^{4+} compound, was recently refined by Mentre and Abraham (1). This oxide, related to the well-known magnetoplumbite family, including $BaFe_{12}O_{19}$ (2), is formed by the connection of four independent vanadium atom coordination polyhedra. $V(1)O_6$ octahedra are edge shared to give rise to layers parallel to the (a, b) plane. V(2) and V(3) form face-sharing V_2O_9 dimers while V(4) is displaced from the center of a trigonal bipyramid. Finally, $V(2)V(3)O_9$ and $V(4)O_5$ bridge layers. Therefore, this oxide retains an acentric $P6_3mc$ space group while other compounds of this family such as NaV_6O_{11}, SrV_6O_{11} (3), or $BaFe_4Ti_2O_{11}$ (4, 5) always crystallize at room temperature with the centrosymmetric $P6_3/mmc$ space group. The reduction of symmetry was assigned to the Pb^{2+} $6s^2$ lone pair effect and is at the basis of the strong magnetic frustration arising in the layered Kagomé-type sublattice of the *R* blocks. It is noteworthy that $BaSn_2Fe_4O_{11}$ was first considered to adopt the $P6_3/mmc$ space group (5); however, a subsequent study revealed a slightly different (orthorhombic *Cmcm*) structure with a twice as large unit cell and somewhat different cationic arrangement (6). Pure PbV_6O_{11} materials cannot be obtained in our conditions of synthesis because it is always assorted with appreciable amounts of $Pb_{1.32}V_{8.35}O_{16.7}$ (1). Single crystals of this accompanying hollandite type Pb–V–O oxide were initially isolated from a mixture of the two compounds (1). A later study permitted the preparation of single phase lead–vanadium *R*-block oxide by the partial substitution of Fe^{3+} for V^{3+}, leading to the $PbFe_xV_{6-x}O_{11}$ series, $1 \leq x \leq 1.75$. Several other cations (Ti^{4+}, Cr^{3+}, Sn^{2+}) were also tested but appear to lead preferentially to hollandite-like compounds (7). Fe^{3+} substituted compounds conserve the structural characteristics of PbV_6O_{11} as confirmed by the structural refinement of $PbFe_{1.75}V_{4.25}O_{11}$ by single crystal X-ray diffraction and so allow the investigation of the PbV_6O_{11} analog physical properties (electric and magnetic) (7). Correlations between

[1] To whom correspondence should be addressed.

0022-4596/99 $30.00

magnetic and electric properties were indicated by a spin-frustrated/insulator → paramagnetic/semiconductor transition. Furthermore Fe^{3+}/V^{3+}–V^{4+} ordering is observed since the X-ray crystal structure of $PbFe_{1.75}V_{4.25}O_{11}$ seems to indicate a strong preference of Fe^{3+} species for the $M(4)$ triangular bipyramidal site while $M(1)$ interstices of the octahedral layers are solely occupied by vanadium cations. As a matter of fact, the dimeric $M(2)$ and $M(3)$ crystallographic positions appeared to accomodate both iron and vanadium cations. In order to determine the site preference of the transition metal in its crystallographic positions we have performed a complete room-temperature study by both powder neutron diffraction and ^{57}Fe Mössbauer spectroscopy on four compositions of the $PbFe_xV_{6-x}O_{11}$ series. The quasi transparent behavior of vanadium towards neutrons, $b_V = -0.038 \cdot 10^{-12}$ cm, and the rather different environment of the four independent Fe/V sites make these two methods suitable on this investigation. In addition, this paper deals with the main results of the low-temperature study including crystal structure and possible magnetic structure.

EXPERIMENTAL

Synthesis

$PbFe_xV_{6-x}O_{11}$ samples were prepared over the 1–1.75 x range as black polycrystalline powders from $Pb_2V_2O_7$, Fe_2O_3, and V_2O_3 mixed in a $1/2{:}x/2{:}(5-x)/2$ molar ratio. Pressed pellets were heated at 850°C for 3 days in evacuated silica tubes. $Pb_2V_2O_7$ was previously prepared by annealing a 2:1 molar ratio of PbO and V_2O_5 at 600°C in air for 3 days. V_2O_3 was obtained by reducing V_2O_5 under flowing hydrogen at 850°C. Because of the large quantity of materials required for neutron experiments, about 6 g of each phase was prepared for $x = 1$, 1.25, 1.5, and 1.75 compositions. Purity was checked using a Siemens D 5000 X-ray diffractometer (Cu$K\alpha$ radiation). For $x = 1$, 1.25, and 1.5, amounts of iron substituted $Pb_{1.32}V_{8.35}O_{16.7}$ were found to be present. For $x = 1.75$, the prepared oxide is accompanied by Fe_2O_3 as an impurity. Actually, one should conclude that $PbFe_xV_{6-x}O_{11}$ phases can be solely obtained in small quantity as reported in (7), while the achievement of the reaction from a large starting charge is not completed.

Neutron Data Collection and Structure Refinement

In many magnetoplumbite related materials such as $BaFe_{12-2x}Co_xSn_xO_{19}$ (8), $BaFe_{12-2x}Co_xTi_xO_{19}$ (9), or $LaZnFe_{11}O_{19}$ (10), cationic distribution was studied using a wide variety of methods such as apparent valencies calculations, Mössbauer spectroscopy or neutron diffraction. Because of the reasons stated in the Introduction, neutron diffraction appears as the most efficient method in our case. The neutron diffraction data were collected with the high-resolution D1A powder diffractometer of the Institut Laue Langevin (ILL) at Grenoble, France, at 300 and 2 K with $\lambda = 1.911$ Å. Rietveld refinement was applied using the FULLPROF 97 (11) program. The room temperature collection conditions, profile fitting parameters, and final reliability factors are given in Table 1.

The pattern matching was first fitted considering the above noted second phase. The 0–10° and 150–160° limit regions were excluded because they were not informative. For $x = 1.75$, two supplementary domains 45.98–46.70° and 53.48–54.68° corresponding to weak unidentified lines were also extracted. Even if powder diffraction cannot distinguish between Friedel pairs that are not equivalent in $P6_3mc$, our attempts in $P63/mmc$ did not converge providing large thermal ellipsoids around lead atoms The crystal structures were refined in the $P6_3mc$ space group using the $PbFe_{1.75}V_{4.25}O_{11}$ single crystal results (7) as starting values. This essentially consisted of refining the Fe/V occupancy in the four independent transition metal sites. The isotropic thermal coefficients were considered for Pb and oxygen atoms. The thermal factors for the mixed sites were fixed at the 0.5 $Å^2$ value in order to perform a good refinement of occupancies. In the last runs, the following parameters were refined: zero, unit-cell, half-width, pseudo-Voigt, and asymmetry parameters for the peak shape, positional, thermal, and occupancy for the crystal structure. The final atomic coordinates and isotropic thermal factors at 290 K are listed in Table 2. Interatomic distances are reported and compared with those of PbV_6O_{11} in Table 3. Taking account of the presence of impurities, the refined occupancies are in good accordance with the expected stoichiometry, leading to $PbFe_1V_5O_{11}$, $PbFe_{1.21}V_{4.79}O_{11}$, $PbFe_{1.6}V_{4.4}O_{11}$, and $PbFe_{1.75}V_{4.25}O_{11}$ formulae. The $x = 1.75$ sample 2 K pattern was also refined considering the extra magnetic phase. The good agreement between the observed and the calculated profiles of the patterns is shown in Fig. 1 for the $x = 1.21$ compound.

Mössbauer Spectroscopy

^{57}Fe Mössbauer studies were performed at 300 and 77 K by using the classical method with ^{57}Co source diffused into a rhodium matrix. The samples previously used for the structural and magnetic investigations were mixed with boron nitride and spread out in a sample holder with a surface of 3 cm^2; it contained about 5 mg of natural iron per cm^2. The Mössbauer spectra were fit using the MOSFIT program (12).

RESULTS AND DISCUSSION

Rietveld Refinement

Powder neutron diffraction study showed a statistical iron occupancy of selected crystallographic sites assorted

TABLE 1
Conditions of Neutron Data Collection and Rietveld Refinement Results for $PbFe_xV_{6-x}O_{11}$ ($x = 1$, 1.21, 1.6, 1.75)

	Data collection			
Diffractometer	ILL D1A			
Wavelength	1.911 Å, monochromator Ge115			
2θ range	0–160			
Step scan	0.05			
Time/step	12 h (accumulation time)			
	Crystallographic data			
System	Hexagonal			
Space group	$P6_3mc$			
Z	2			
	Results of Rietveld refinement			
	$PbFe_1V_5O_{11}$	$PbFe_{1.21}V_{4.79}O_{11}$	$PbFe_{1.6}V_{4.4}O_{11}$	$PbFe_{1.75}V_{4.25}O_{11}$
Cell parameters	$a = 5.7428(1)$	$a = 5.7413(1)$	$a = 5.7416(1)$	$a = 5.7414(1)$
	$c = 13.4372(2)$	$c = 13.4626(2)$	$c = 13.4916(2)$	$c = 13.5094(2)$
Volume (Å^3)	383.8	384.3	385.2	385.7
Number of reflections	107	102	102	102
Number of refined parameters	37	37	37	35
Zero-point ($^\circ 2\theta$)	−0.035(1)	−0.060(1)	−0.048(1)	−0.049(1)
Profile function		Pseudo-Voigt		
	$\eta = 0.19(1)$	$\eta = 0.14(1)$	$\eta = 0.10(1)$	$\eta = 0.16(1)$
Halfwidth parameters	$U = 0.126(4)$	$U = 0.125(4)$	$U = 0.099(3)$	$U = 0.115(4)$
	$V = -0.242(8)$	$V = -0.198(6)$	$V = -0.198(6)$	$V = -0.222(8)$
	$W = 0.210(3)$	$W = 0.181(3)$	$W = 0.181(3)$	$W = 0.195(3)$
Asymmetry parameters	0.09(3)–0.03(1)	0.13(3)–0.04(1)	0.15(3)–0.05(1)	0.17(2)–0.05(1)
R_{wp}	5.80	5.87	5.89	5.74
R_p	4.33	4.42	4.46	4.35
R_F	3.82	4.69	6.03	5.47
R_{Bragg}	3.68	4.25	5.33	5.42
χ^2	2.77	3.11	3.25	4.70

$R_{wp} = [\sum_i w_i (y_i - y_{ci})^2 / \sum_i w_i y_i^2]^{1/2}$; $R_p = \sum_i |y_i - y_{ci}| / \sum_i y_i$;
$R_F = \sum ||F_{obs}|| - ||F_{calc}|| / \sum |F_{obs}|$; $R_{Bragg} = \sum |I_k - I_k^{calc}| / \sum I_k$
$\chi^2 = [R_{wp}/R_{exp}]^2$

with the distortion of some polyhedra. The most outstanding feature is the already observed off-centering of Pb^{2+} within its cuboctahedron cage related to the $P6_3mc$ space group (1, 7). This effect remains constant in the $PbFe_xV_{6-x}O_{11}$ series with Pb–O(1)/opposite Pb–O(3) distances ranging from 2.485(13)/3.036(14) for PbV_6O_{11} to 2.599(7)/3.063(7) for $PbFe_{1.75}V_{4.25}O_{11}$. Hence, Pb^{2+} is displaced 0.35 Å parallel to the c axis from the pseudomirror plane containing the O(2) atoms in PbV_6O_{11} while in the substituted phases, this displacement corresponds to 0.31, 0.34, 0.27, and 0.27 Å for $x = 1$, 1.21, 1.6, and 1.75, respectively.

Figure 2 shows the crystal structure and iron occupancies n the whole unit cell. The different site occupancies for mixed-cationic compounds in the various crystallographic sites are shown in Table 4 for several R-block iron substituted compounds. Our results clearly show that from the lowest substitution rates, Fe^{3+} preferentially occupies the bipyramidal $M(4)$ site until a maximum occupancy of 64% is reached for $PbFe_{1.6}V_{4.4}O_{11}$. This result partially refutes our previously reported $PbFe_{1.75}V_{4.25}O_{11}$ crystal structure assigning 100% occupancy of the $M(4)$ site by iron (7), but still explains the sudden increase of the c parameter as compared PbV_6O_{11} ($c = 13.267(3)$ Å) to $PbFe_1V_5O_{11}$ ($c = 13.4372(2)$ Å). The Fe^{3+} introduction effect on the c parameter was described in (7). $M(4)$ species are displaced from the equatorial $O(2)_3$ plane toward the O(4) apex. This displacement is emphasized for Fe^{3+} imparting a pseudotetrahedral character to $M(4)$. It exaggerates the $O(2)_3$–$M(4)$ shift from 0.17 Å for PbV_6O_{11} to nearly equal 0.34, 0.31, 0.34, and 0.29 Å for $x = 1$, 1.21, 1.6, and 1.75, respectively. This displacement is responsible for longer opposite apical distances $M(4)$–O(5) than those seen with PbV_6O_{11}, even if the three short equatorial bonds $M(4)$–O(2) (1.82 Å in substituted phases) are nearly equal to the corresponding V(4)–O(2) bonds (1.826(7) Å) in PbV_6O_{11}. This result is in agreement with the related structure $SrFeV_5O_{11}$ as determined by Rietveld refinement of its neutron powder pattern

TABLE 2
Refined Atomic Parameters and Fe/V Occupancy for $PbFe_1V_5O_{11}$ (*a*), $PbFe_{1.21}V_{4.79}O_{11}$ (*b*), $PbFe_{1.6}V_{4.4}O_{11}$ (*c*), $PbFe_{1.75}V_{4.25}O_{11}$ (*d*)

Atom	Site	Occupancy	*x*	*y*	*z*	*B* (Å^2)
	a				0.2270(4)	1.7(1)
Pb	2(*b*) *b*	1	1/3	2/3	0.2243(5)	2.21(11)
	c				0.2296(4)	2.18(11)
	d				0.2302(4)	1.77(11)
	a	1/0	0.509(2)	−0.509(2)	−0.015(3)	
V(1)/Fe(1)	6(*c*) *b*	0.99(1)/0.01(1)	0.513(3)	−0.513(3)	0.009(4)	0.5
	c	0.97(3)/0.03(3)	0.511(3)	−0.511(3)	−0.002(5)	
	d	0.95(1)/0.05(1)	0.510(3)	−0.510(3)	−0.002(5)	
	a	0.70(2)/0.30(2)			0.141(1)	
V(2)/Fe(2)	2(*a*) *b*	0.59(1)/0.41(1)	0	0	0.133(1)	0.5
	c	0.58(2)/0.42(2)			0.155(2)	
	d	0.38(1)/0.62(1)			0.155(1)	
	a	0.84(2)/0.16(2)			0.348(3)	
V(3)/Fe(3)	2(*a*) *b*	0.73(2)/0.27(2)	0	0	0.342(2)	0.5
	c	0.55(2)/0.45(2)			0.365(1)	
	d	0.58(1)/0.42(1)			0.370(8)	
	a	0.46(1)/0.54(1)			0.276(5)	
V(4)/Fe(4)	2(*b*) *b*	0.49(1)/0.51(1)	2/3	1/3	0.273(1)	0.5
	c	0.36(1)/0.64(1)			0.275(1)	
	d	0.44(1)/0.56(1)			0.272(6)	
	a		0.1750(5)	−0.1750(5)	0.0765(4)	0.58(7)
O(1)	6(*c*) *b*	1	0.1721(5)	−0.1721(5)	0.0782(1)	0.95(8)
	c		0.1729(5)	−0.1729(5)	0.0786(4)	0.54(7)
	d		0.1742(5)	−0.1742(5)	0.0776(5)	0.87(8)
	a		0.1527(4)	−0.1527(4)		0.69(8)
O(2)	6(*c*) *b*	1	0.1536(4)	−0.1536(4)	3/4	0.96(8)
	c		0.1534(3)	−0.1534(3)		0.74(7)
	d		0.1534(3)	−0.1534(3)		0.84(8)
	a		0.1683(6)	−0.1683(6)	0.4219(4)	0.27(8)
O(3)	6(*c*) *b*	1	0.1718(5)	−0.1718(5)	0.4205(4)	0.50(8)
	c		0.1717(5)	−0.1717(5)	0.4206(4)	0.49(8)
	d		0.1713(4)	−0.1713(4)	0.4230(4)	0.13(7)
	a				0.4137(5)	0.61(13)
O(4)	2(*b*) *b*	1	2/3	1/3	0.4130(5)	0.72(13)
	c				0.4158(6)	0.28(10)
	d				0.4120(5)	0.18(10)
	a				0.0883(6)	1.17(15)
O(5)	2(*b*) *b*	1	2/3	1/3	0.0868(6)	0.60(14)
	c				0.0858(6)	0.30(14)
	d				0.0862(6)	0.29(14)

by Kanke *et al.* (13), which revealed a 56% iron occupancy for the same site. This preferential Fe(4) localization is inherent to the Fe^{3+} species. Although this cation is readily accomodated in a tetrahedral, triangular bipyramidal, or octahedral coordination, Fe^{2+}/Fe^{3+} solely fill the tetrahedral [A] subarray of the $Fe[V_xFe_{2-x}]O_4$ spinel, whatever the postulated distribution (14). A neutron powder diffraction study (5) indicated that the *M*(4) sites of $BaTi_2Fe_4O_{11}$ and $BaSn_2Fe_4O_{11}$ are occupied by Fe^{3+} ions exclusively, suggesting potentially the same results for $PbFe_xV_{6-x}O_{11}$, $x \geq 4$, materials that we did not obtain as single phases.

Furthermore, iron atoms indicate a statistical occupancy in the *M*(2) and *M*(3) dimeric octahedra sites which increases from 30 and 16% ratio for $x = 1$ to 62 and 42.5% ration for $x = 1.75$. Such an occupancy leads to an electrostatic repulsion between the *M*(2) and the *M*(3) dimeric octahedra cations which increases with iron substitution: *M*(2)–*M*(3) = 2.72(3), 2.78(5), 2.81(2), 2.82(3), and 2.90(1) Å for $x = 0$, 1, 1.21, 1.6, and 1.75, respectively. This phenomenon cannot be explained in terms of ionic radii since six-coordinated high spin Fe^{3+} (0.64 Å) has an ionic radius comparable to that of six-coordinated V^{3+}(0.64 Å) (15). By contrast, a more efficient electrostatic repulsion from peripheral d^5 electrons of Fe^{3+} ions versus those of d^1 (V^{4+}) and d^2 (V^{3+}) might be considered. The existence of a V(2)–V(3) metal–metal bonding that would be weakened by iron as an impurity can also be suggested. The dimeric *M*(2)–*M*(3) sites adopt a mixed content in all of the presented examples, Table 4.

Finally, powder neutron diffraction performed on substituted phases and single-crystal X-ray diffraction refinement for $PbFe_{1.75}V_{4.25}O_{11}$ are in excellent agreement concerning the *M*(1) octahedral layers that are almost solely occupied by vanadium atoms for the four studied compositions. $SrFeV_5O_{11}$ behaves similarly. As observed in $SrTiV_5O_{11}$, $SrTi_{1.5}V_{4.5}O_{11}$, and $SrCrV_5O_{11}$, other doping cations such as Cr^{3+} and Ti^{4+} can be slightly accommodated by the *M*(1) site that always conserves a major vanadium load (13). Valence sum calculations are not suitable for mixed sites and were not performed on *M*(2), *M*(3), and *M*(4) sites but only on the *M*(1) octahedra layers using Brown and Altermatt (16) data for V^{3+} and V^{4+} cations. The results are given in Table 5. They indicate a mixed V^{3+}/V^{4+} valence within the layers in contrast to SrV_6O_{11}, NaV_6O_{11} (3), and PbV_6O_{11} (1), which mostly accommodate V^{3+} in the V(1) layers.

Mössbauer Spectroscopy

Mössbauer spectra obtained at room temperature for the $PbFe_xV_{6-x}O_{11}$ series are shown in Fig. 3. The refined values of the hyperfine parameters are reported in Table 6.

These spectra reveal that the hyperfine structure is similar for the four compositions and results only from the presence of pure electric interactions. Each of them has been well reproduced by considering at least four quadrupole components of iron, labeled 1, 2, 3, and 4 in Table 6.

— Contribution 1 presents an isomer shift value relative to Fe–metal, which is, particularly for $x = 1$ and 1.25 (IS = 0.55 mm/s), too high for trivalent high spin iron and

TABLE 3
Main Metal–Oxygen Distances (Å) in $PbFe_xV_{6-x}O_{11}$ ($x = 0$–1–1,25–1,5–1,75) Phases from Neutron Rietveld Refinement

	PbV_6O_{11} from ref. (1)	$PbFe_1V_5O_{11}$	$PbFe_{1.21}V_{4.79}O_{11}$	$PbFe_{1.6}V_{4.4}O_{11}$	$PbFe_{1.75}V_{4.25}O_{11}$ 290 K/2 K
M(1) environment					
2 *M*(1)–O(1)	1.983(9)	2.073(25)	1.943(31)	2.007(40)	1.992(40)/2.0(2)
2 *M*(1)–O(3)	1.913(9)	1.815(21)	1.967(36)	1.892(40)	1.881(39)/1.9(2)
1 *M*(1)–O(4)	2.114(9)	1.992(22)	2.200(36)	2.081(40)	2.111(40)/2.0(2)
1 *M*(1)–O(5)	1.998(10)	2.096(27)	1.857(35)	1.955(44)	1.956(44)/2.0(2)
M(2) environment					
3 *M*(2)–O(1)	1.971(9)	1.942(9)	1.865(7)	2.008(12)	2.025(7)/2.001(10)
3 *M*(2)–O(2)	2.053(8)	2.114(14)	2.191(10)	1.998(14)	1.992(7)/2.001(10)
M(3) environment					
3 *M*(3)–O(2)	2.007(8)	2.010(30)	1.970(13)	2.173(14)	2.229(8)/2.166(14)
3 *M*(3)–O(3)	1.924(9)	1.947(24)	2.006(11)	1.868(8)	1.846(5)/1.861(9)
M(4) environment					
3 *M*(4)–O(2)	1.826(7)	1.830(3)	1.814(3)	1.821(2)	1.814(2)/1.822(3)
1 *M*(4)–O(4)	1.960(16)	1.853(10)	1.882(11)	1.894(10)	1.890(10)/1.93(1)
1 *M*(4)–O(5)	2.259(16)	2.519(11)	2.509(11)	2.558(11)	2.511(11)/2.52(1)
Pb environment					
3 Pb–O(1)	2.485(12)	2.563(7)	2.537(7)	2.587(7)	2.599(7)/2.575(8)
6 Pb–O(2)	2.903(4)	2.891(2)	2.894(2)	2.887(2)	2.886(2)/2.885(3)
3 Pb–O(3)	3.036(13)	3.091(7)	3.092(7)	3.038(7)	3.063(7)/3.086(8)

Note. For $x = 1.75$, distances are given for both the 290 and 2 K studies. PbV_6O_{11} distances were refined from single-crystal X-ray diffraction, Ref. (1).

too low for divalent iron. It can be attributed to an average oxidation state of 2.75. The quadrupole splitting values are very low and the relative proportion of this contribution remains constant for $x > 1$.

— Contributions 2 and 3 have very similar IS values (0.4 mm/s), higher than that of site 1, and quadrupole splitting values which both give evidence for sixfold coordinated trivalent iron (17). All these parameters are independent of x.

— The last contribution, labeled 4, corresponds to an iron site with a low value of the isomer shift, in agreement with that observed in other high spin Fe^{3+} oxides (18) and a high value of the quadrupole splitting compared to the preceeding contributions.

Using the results of our present neutron investigations, we can now discuss the partitioning of iron atoms in the different sites and compare them with previous Mössbauer results obtained in studies of other oxides with *R*-type hexagonal structure (4, 5).

The neutron diffraction results clearly show that the Fe^{3+} preferentially occupy the bipyramidal *M*(4) site and progressively and statistically the dimeric octahedra *M*(2) and *M*(3), with the *M*(1) site being preferentially a vanadium position.

Thus, we can consider that the Mössbauer site (4), which is the most populated, can be attributed to the *M*(4) site. On the other hand, we know that the lowest isomer shift value for a trivalent iron ion (0.30 mm/s for this site) corresponds to the lowest degree of coordination (18). In our compound, this lowest degree is observed for the pentacoordinated bipyramidal site, at variance from the others, which are in octahedral positions. The high QS value (1.27 mm/s) indicates a high asymmetry of the environment which can be influenced by the presence of the lone pair near this site.

Sites 2 and 3 which present intensity ratios very close to those obtained by neutron diffraction and typical for iron octahedral sites (19) can be attributed to the *M*(2) and *M*(3) sites.

For site 1, Mössbauer and neutron data are in agreement only for $x = 1.75$. For $x < 1.6$, failure to agree is due to the presence in the compounds of impurities, as evidenced by neutron diffraction, which can give a Mössbauer contribution corresponding to a high value of IS.

If we consider the hyperfine parameters obtained for different sites in other related structures, e.g., $BaFe_4Ti_2O_{11}$ (4), we can observe a good agreement for the IS (relative to Fe–metal) and QS values. However, the largest QS value is observed for the 4*f* position in the barium compound compared to that of the equivalent *M*(4) site.

Low Temperature Crystal Structure

In order to access the possible magnetic structure of $PbFe_{1.75}V_{4.25}O_{11}$, its neutron diffraction pattern was collected at 2 K. The nuclear phase crystal structure was

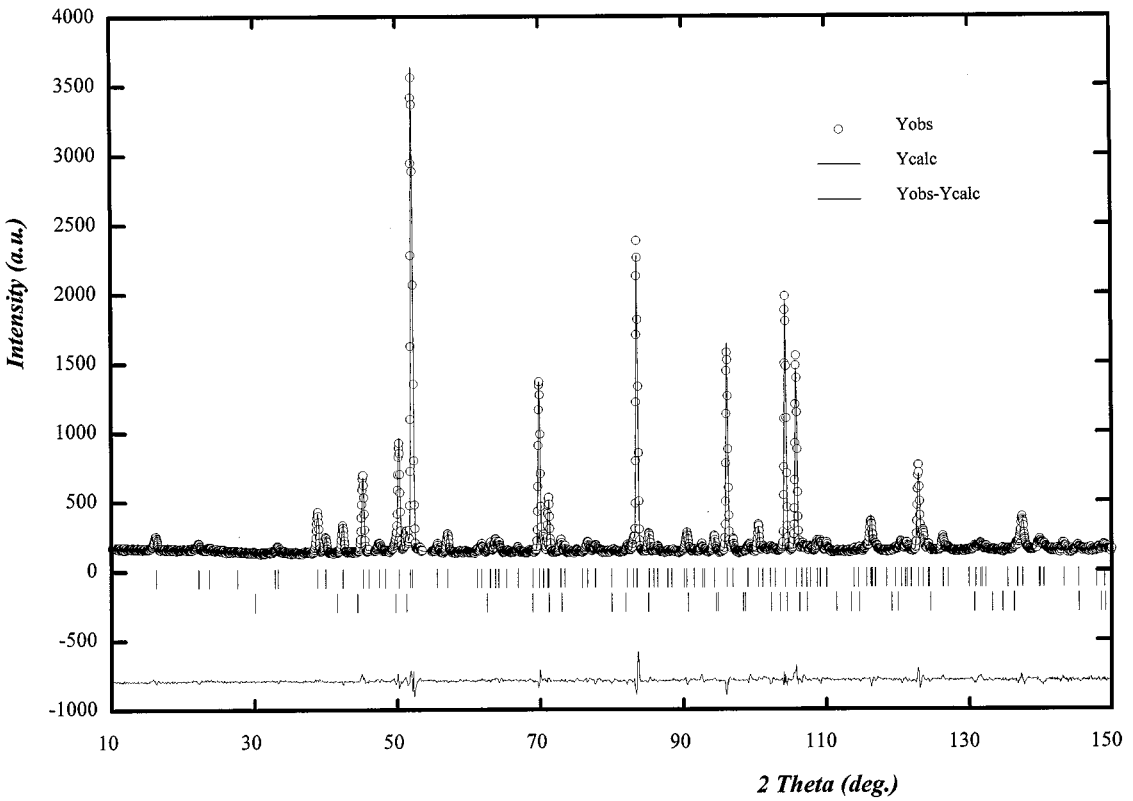

FIG. 1. Observed and calculated neutron diffraction profile for $x = 1.21$ at 290 K. A difference curve appears at the bottom of the figure.

refined from room temperature results. One must notice the expected contraction of the a unit cell parameter, $a_{2K} = 5.7261(2)$ Å, while c astonishingly increases by lowering the temperature with $c_{2K} = 13.5579(3)$ Å. The crystal structure was satisfactorily refined in the $P6_3mc$ space group in contrast to NaV_6O_{11} that undergoes a two-step second order–one order structural phase transition upon cooling: hexagonal $(P6_3/mmc) \rightarrow$ hexagonal $(P6_3mc) \rightarrow$ orthorhombic ($Cmc2_1$) at 245 and 35–40 K (20, 21). Fixing the Fe/V displayed at 290 K, the final atomic parameters and reliability factors are given in Table 7 and show a nearly unchanged arrangement. One can notice the Pb temperature factor lowering while M–O distances remain the same for the two temperatures. Only the $M(3)$ and $M(4)$ environments are sensibly modified, the apical $M(4)$–O(4) and $M(4)$–O(5) elongations supporting the c increase.

TABLE 4
Relative Transition Metal Occupancies in the Available Crystallographic Sites for Several AM_6O_{11} Oxides

	$BaTi_2Fe_4O_{11}$[a]	$BaSn_2Fe_4O_{11}$[a]	$SrTiV_5O_{11}$[b]	$SrTi_{1.5}V_{4.5}O_{11}$[b]	$SrCrV_5O_{11}$[b]	$SrFeV_5O_{11}$[b]
$M(1)$	65% Fe, 35% Ti	74% Fe, 26% Sn	12% Ti, 88% V	13% Ti, 87% V	15% Cr, 85% V	100% V
$M(2)$[c]	52% Fe, 48% Ti	39% Fe, 61% Sn	24% Ti, 76% V	39% Ti, 61% V	23% Cr, 77% V	24% Fe, 76% V
$M(3)$[c]						
$M(4)$	100% Fe	100% Fe	16% Ti, 84% V	35% Ti, 65% V	7% Cr, 93% V	56% Fe, 44% V
	$PbFe_1V_5O_{11}$		$PbFe_{1.21}V_{4.79}O_{11}$	$PbFe_{1.6}V_{4.4}O_{11}$		$PbFe_{1.75}V_{4.25}O_{11}$
$M(1)$	100% V		98.8% V, 1.2% Fe	96,7% V, 3.3% Fe		95,2% V, 4.8% Fe
(2)	70% V, 30% Fe		59.5% V, 40.5% Fe	58.5% V, 41.5% Fe		38% V, 62% Fe
$M(3)$	84% V, 16% Fe		73.5% V, 26.5% Fe	55.5% V, 44.5% Fe		57.5% V, 42.5% Fe
$M(4)$	46% V, 54% Fe		50% V, 50% Fe	36% V, 64% Fe		44% V, 56% Fe

[a] Ref. (4)
[b] Ref. (16)
[c] In the compounds with the $P6_3/mmc$ space group $M(2)$ and $M(3)$ are equivalent with a doubled multiplicity.

TABLE 5
Valence Bond Sum Calculation for the V(1) Position Using V^{3+} and V^{4+} Data from Ref. (16)

	PbV_6O_{11} [1]	$PbFe_1V_5O_{11}$	$PbFe_{1.21}V_{4.79}O_{11}$	$PbFe_{1.6}V_{4.4}O_{11}$	$PbFe_{1.75}V_{4.25}O_{11}$
V^{3+}	3.06	3.36	3.43	3.28	3.33
V^{4+}	3.42	3.75	3.66	3.66	3.71

Magnetic Features

As we have previously mentioned (7), dc magnetic susceptibility measured following a ZFC-FC process shows a strong onset of irreversibility between 50 and 80 K depending on the x value of $PbFe_xV_{6-x}O_{11}$. This behavior is sufficiently unusual as compared to the ferromagnetic NaV_6O_{11} and metamagnetic SrV_6O_{11} responses (22) to justify further investigations. Figure 4 shows the obtained susceptibility versus T for ZFC/FC cycle measured at 1000 Gauss for $x = 1.75$. The broadness of the peak and crystallographic considerations strongly suggest a freezing phenomenon (7). It is well established that the two essential microscopic ingredients of a spin glass are site disorder and bond frustration (23, 24) which comforts the observed magnetic behavior because of the existing Kagomé sublattice parallel to the (a, b) plane formed by the V(1) atoms. Thus, PbV_6O_{11} homologs are subject to strong bidimensional frustration already observed in the RS type $SrCr_{9x}Ga_{12-9x}O_{19}$ (25, 26). V_3 triangles frustration concept was initially developed for $LiV_{1-y}M_yO_2$ (M = Cr, Ti) and $Li_{1-x}VO_2$ (27) that brings informing features about the question. In the present case, an interacting spin model was previously reported taking account the existence of V_3 trimers in the Kagomé lattice (7). Low temperature hypothesis neutron diffraction experiments were performed on $PbFe_{1.75}V_{4.25}O_{11}$ powder to validate the trial. As shown in Fig. 5, the magnetic contribution appears below 150 K as weak lines superposed on the Bragg peaks, essentially the 100 and 101 magnetic contributions were detected. Thus, long or at least medium magnetic order range arises in the materials. Therefore no satellite peaks were observed on patterns involving the preservation of the nuclear unit cell for the magnetic structure. So, our previously supposed idea based on alterning ferromagnetically ordered and frustrated triangles (7) is partially refuted because of its subsequent a parameter tripling. Furthermore, the weakness of magnetic contributions correlated to the complex crystal structure of R-blocks indicate the difficulty of the refinement that, in the best way, would only lead to a plausible magnetic structure. The refinement problems are increased by the mixed occupancy of magnetic crystallographic sites. The magnetic structure was refined using the FULLPROF 97 and magnetic ions positions and occupancies from the nuclear phase with the spherical coordinates for the magnetic moments (μ, φ, θ). In any case we chose to assign to each atom of the R-block (x, y, z) the same magnetic moment and orientation as its equivalent R^* block ($-y$, $-x$, $\frac{1}{2}+z$). An inversion of the spin direction from R to R^* would drive an AF structure and satellite peaks which are not observed. Triclinic symmetry was used to take into account the $M(1)$ split into three independent $M(1)_{a,b,c}$ atoms. Several different

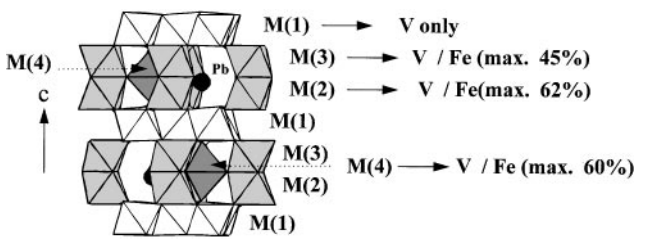

FIG. 2. $PbFe_xV_{6-x}O_{11}$ tridimensional polyhedra assembly and corresponding V/Fe distribution.

TABLE 6
Mössbauer Data for $PbFe_xV_{6-x}O_{11}$ Phases at 300 K

X	Site	I.S.[a] (mm/s) (± 0.01)	Q.S[b]. (mm/s) (± 0.02)	Γ[c] (mm/s) (± 0.02)	% Fe (± 4)	% Fe (neutron) ($> \pm 7$)
1	$M(1)$	0.52	0.32	0.37	20	*0*
	$M(2)$	0.41	0.40	0.22	13	*30*
	$M(3)$	0.40	0.68	0.24	21	*16*
	$M(4)$	0.32	1.27	0.29	46	*54*
1.21	$M(1)$	0.59	0.32	0.32	15	*2.5*
	$M(2)$	0.41	0.40	0.24	25	*33.3*
	$M(3)$	0.39	0.66	0.24	22	*21.7*
	$M(4)$	0.31	1.28	0.27	38	*42.5*
1.6	$M(1)$	0.45	0.21	0.25	13	*5.5*
	$M(2)$	0.42	0.45	0.24	28	*26.4*
	$M(3)$	0.40	0.70	0.24	23	*28.1*
	$M(4)$	0.31	1.29	0.27	36	*40*
1.75	$M(1)$	0.44	0.17	0.26	13	*8.5*
	$M(2)$	0.42	0.41	0.25	24	*35.4*
	$M(3)$	0.39	0.65	0.26	29	*24.1*
	$M(4)$	0.30	1.29	0.28	34	*32.0*

Note. The intensity ratio for each iron site is compared to that obtained from the neutron diffraction data.

[a] I.S., isomer shift relative to Fe metal at 300 K.

[b] Q.S., quadrupolar splitting.

[c] Γ, linewidth at half height.

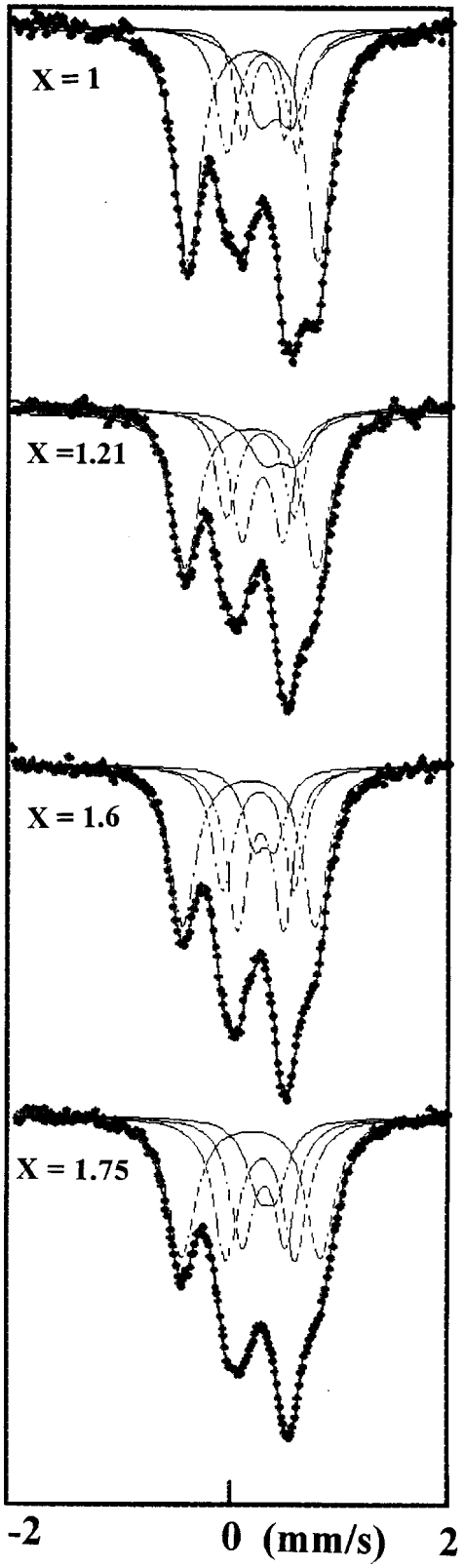

FIG. 3. Mössbauer spectra of $PbFe_xV_{6-x}O_{11}$ with their refined x values at 300 K, with fits of four individual Fe sites.

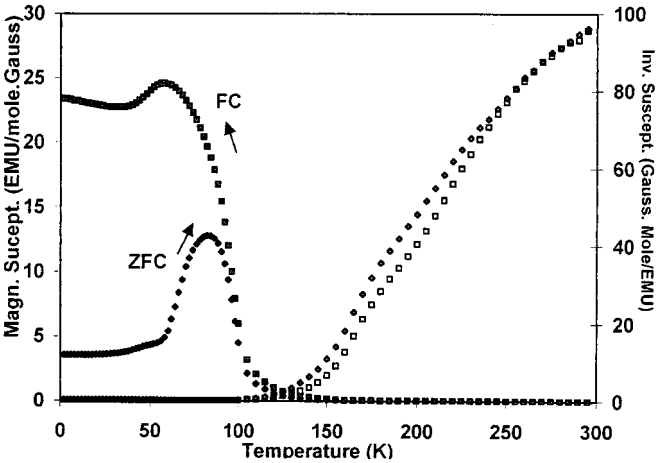

FIG. 4. ZFC/FC susceptibility and inverse susceptibility vs T(K) showing the onset of a strong irreversibility for $PbFe_{1.75}V_{4.25}O_{11}$.

spin models were tested with R_{magn} never lower than 20%. Only two succesful attempts will be described considering their magnetic reliability factor. It is noteworthy that refining the moments for each ion did not converge and a step by step orientation procedure makes it possible to reach a refinement minimum. In the first fair model, $R_{magn} = 13.6\%$, $M(2)$, $M(3)$, and $M(4)$ are assorted with a spin up ↑ parallel to the c axis, while $M(1)a$, $M(1)b$, and $M(1)c$ are ferrimagnetically ordered (two spins up ↑, one spin down ↓). This would lead to a ferrimagnet with c as the easy axis. Furthermore, each independent magnetic moment was refined below its expected values. Therefore, this arrangement remains to be taken in consideration. We preferred to above, a model yielding the same $R_{magn} = 13.6\%$, in which $M(1)_a$, $M(1)_b$, and $M(1)_c$ spins are aligned in the (a, b) plane rotated 120° from each other. $M(2)$, $M(3)$, and $M(4)$ are still assorted with a spin up ↑ (Fig. 6). Nevertheless, the refined μ values

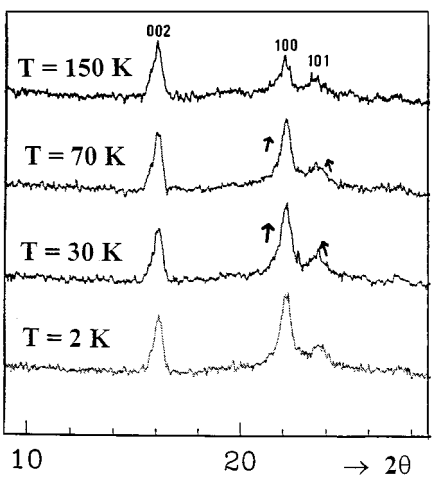

FIG. 5. Low angles 2θ domain for $x = 1.75$; the magnetic contribution weakly appears at 70 K superposed on Bragg peaks.

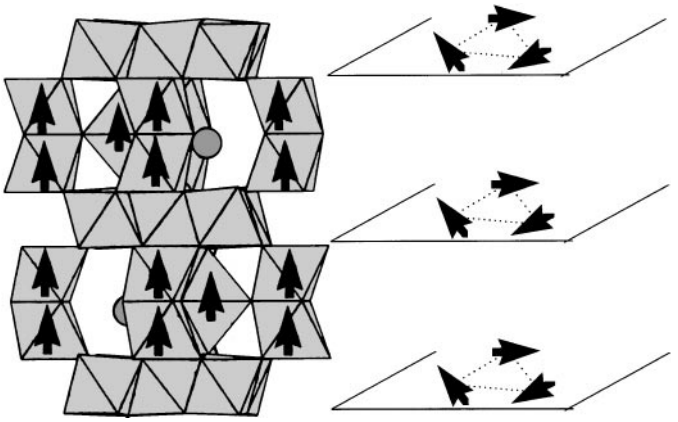

FIG. 6. Refined magnetic structure, $R_{magn} = 13.6\%$ for $x = 1.75$ from the 2 K neutron data.

are very low as compared to the theorical values of 1, 2, and 5 μB for V^{4+}, V^{3+}, and Fe^{3+}, respectively, Table 7. This model displays a strong frustration over the $M(1)$ Kagome sublattice. The calculated magnetic intensities of $00l$ reflexions are calculated to null be despite the Kagome lattice momentum perpendicular to their scattering vectors. A medium range order could justify the low value refined for the magnetic moments. The refinement of an average magnetic moment for all $M(1)$, $M(2)$, $M(3)$ and $M(4)$ species yield $\mu_{global} = 1.063$ μB. Low temperature Mössbauer spectroscopy and ac susceptibility measurements are currently under investigation to comfort our results.

TABLE 7

Refined Atomic Coordinates and Spin Moment (μ_1 for average V^{3+}/V^{4+} and μ_2 for Fe^{3+}) and Orientation for the Magnetic Phase of $PbFe_{1.75}V_{4.25}O_{11}$ at 2 K

	x	y	z	Spin	μ_1/μ_2
V(1)*a*	0.511(3)	−0.511(3)	−0.004(4)	△‾	0.3(1)/1.06(9)
V(1)*b*	0.511(3)	1.022(3)	−0.004(4)	△/	0.3(1)/1.06(9)
V(1)*c*	−0.022(3)	−0.511(3)	−0.004(4)	\△	0.3(1)/1.06(9)
V(2)/Fe(2)	0	0	0.153(1)	↑	2.01(9)/1.06(9)
V(3)/Fe(3)	0	0	0.364(1)	↑	0.4(1)/1.06(9)
V(4)/Fe(4)	2/3	1/3	0.274(1)	↑	0.8(1)/1.06(9)

Note. △, Spins are aligned parallel to the (a, b) plane and turned 120° from each other. μ_1 and μ_2 are the refined magnetic moment independently and with a same value for all positions, respectively.

ACKNOWLEDGMENTS

The authors gratefully acknowledge the ILL facilities and staff for the neutron diffraction experiments and especially Emmanuelle Suard for help and advice during the data collection.

REFERENCES

1. O. Mentre and F. Abraham, *J. Solid State Chem.* **125,** 91 (1996).
2. X. Obradors, A. Collomb, M. Pern, D. Samaras, and J. C. Joubert, *J. Solid State Chem.* **56,** 171 (1985).
3. Y. Kanke, K. Kato, E. Takayama-Muromachi, and M. Isobe, *Acta Crystallogr.* **C48,** 1376 (1992).
4. X. Obradors, A. Collomb, J. Pannetier, A. Isalgue, J. Tejada, and J. C. Joubert, *Mater. Res. Bull.* **18,** 1543 (1983).
5. M. C. Cadee and D. J. W. Ijdo, *J. Solid State Chem.* **52,** 302 (1984).
6. M. Shiojiri, *Joel News* **26E,** 2 (1988).
7. O. Mentre, A. C. Dhaussy, F. Abraham, and H. Steinfink, *J. Solid State Chem.* **130,** 223 (1997).
8. F. Sandiumenge, B. Martinez, X. Battle, S. Gali, and X. Obradors, *J. Appl. Phys.* **72,** 4608 (1992)
9. M. V. Cabanas, J. M. Gonzalez-Calbet, J. Rodriguez-Carjaval, and M. Vallet-Regi, *J. Solid State Chem.* **111,** 229 (1994).
10. X. Obradors, A. Isalgue, A. Collomb, M. Pernett, J. A. Pereda, J. Tejada, and J. C. Joubert, *J. Phys C: Solid State Phys.* **19,** 6605 (1986).
11. J. Rodriguez-Carjaval, FULLPROF 97, Laboratoire Leon Brillouin (CEA-CNRS), France, 1997.
12. J. Teillet and F. Varret, Program MOSFIT, unpublished.
13. Y. Kanke, F. Izumi, E. Takayama-Muromachi, K. Kato, T. Kamiyama, and H. Asano, *J. Solid State Chem.* **92,** 261 (1991).
14. C. Gleitzer and J. B. Goodenough, *in* "Mixed Valence Iron Oxides," "Structure and Bonding." Springer-Verlag, Berlin/Heidelberg, 1985.
15. R. D. Shannon, *Acta Crystallogr. Sect. A* **32,** 751 (1976).
16. I. D. Brown and D. Altermatt, *Acta Crystallogr. Sect. B* **41,** 244 (1985).
17. L. Permer, Y. Laligant, G. Ferey, and Y. Calage, *J. Solid State Chem.* **107,** 539 (1993)
18. N. M. Greenwood and T. C. Gibb, "Mössbauer Spectroscopy," p. 259. Chapman & Hall, London, 1971.
19. N. Nguyen, Y. Calage, F. Varret, G. Ferey, V. Caignaert, M. Hervieu, and B. Raveau, *J. Solid State Chem.* **53,** 398 (1984).
20. Y. Kanke, F. Izumi, Y. Morii, E. Akiba, S. Funahashi, K. Kato, M. Isobe, E. Takayama-Muromaci, and Y. Uchida, *J. Solid State Chem.* **112,** 429 (1994).
21. M. Iwata and Y. Ishibashi, *J. Phys. Soc. Jpn.* **67,** 691 (1998).
22. Y. Uchida, Y. Kanke, and Y. Onoda, *in* "Proceedings 6th International Conference on Ferrites, Tokyo, 1992," p. 722.
23. K. Binder and A. P. Young, *Rec. Mod. Phys.* **58,** 801 (1986).
24. K. H. Fisher, *Phys. Status Solidi B* **116,** 357 (1983); **130,** 13 (1985).
25. A. P. Ramirez, G. P. Espinosa, and A. S. Cooper, *Phys. Rev. B* **45,** 2505 (1992).
26. S-H. Lee, C. Broholm, G. Aeppli, T. G. Perring, B. Hessen, and A. Taylor, *Phys Rev. Lett.* **76,** 4424 (1996).
27. J. B. Goodenough and A. Manthiram, *Phys. Rev. B* **43,** 10170 (1990).